

Development of a Full Human Body Finite Element Model for Blunt Injury Prediction Utilizing a Multi-Modality Medical Imaging Protocol

F. Scott Gayzik^{1,2}, Daniel P. Moreno^{1,2}, Nicholas A. Vavalle^{1,2}, Ashley C. Rhyne^{1,2},
Joel D. Stitzel^{1,2}

1. Wake Forest University School of Medicine
2. Virginia Tech – Wake Forest Center for Injury Biomechanics

Abstract

Computational modeling is an increasingly important tool in the study of injury biomechanics. This paper describes the development and validation of a seated human body finite element model as part of the Global Human Body Models Consortium (GHBMC) project. The model was developed using LS-DYNA[®] (LSTC, Livermore, CA) and is intended for blunt injury prediction. The geometry of the model is based on a protocol that leverages the strengths of three clinical scanning methods; computed tomography (CT), magnetic resonance imaging (MRI), and upright MRI (i.e. subject in seated position). The protocol was applied to a living male volunteer (26 years, height, 174.9 cm, and weight, 78.6 kg) who met extensive anthropometric and health criteria. Computer Aided Design (CAD) data were developed from the images, containing significant anatomical detail. Seventeen sub-substructures of the brain, 52 muscles of the neck, and all major organs of the thorax and abdomen, with associated vasculature, are represented in finite element model. The positioning of the axial skeleton and the location of organs were determined using upright MRI scans to represent the seated posture.

A region-specific development approach was used, with five Body Region Centers of Expertise (COEs) focused on meshing and regional validation of the head, neck, thorax, abdomen, pelvis and lower extremity. The regional models were then integrated into a full body model. Mesh connections between neighboring body regions were assembled using techniques based on the geometry, element type, and anatomic purpose. This consisted of nodal connections for all 1-D beam and discrete element connections (e.g. ligamentous structures), 2D shells (e.g. the inferior vena cava to right atrium), and many 3D tetrahedral and hexahedral structures (e.g. soft tissue envelope connections between body regions). In cases where node-to-node connections were not made, (e.g. 3D muscle to bone insertions), contact definitions were implemented.

The integrated full body model consists of 1.3 million nodes, and 1.9 million elements. Element types in the model are 41.0 % hexahedral, 33.8 % tetrahedral, 19.5 % quad shell, 5.1% tri shell, and 0.6 % others including beam and discrete elements. Non-linear and/or viscoelastic material models were used where appropriate. Simulations were conducted using MPP LS-DYNA R.4.2.1. The model has been validated against a number of frontal and lateral rigid impactor and sled tests. Two of these (a chest impact per Kroell and an abdominal impact per Hardy) are highlighted via computational benchmarking on a computational cluster running Red Hat Enterprise Linux 4.0. Benchmarking tests ranged from 8 to 88 nodes. Reductions in compute times are seen up to 80 CPUs. Using 64 CPUs, solution times for the 60 ms chest impact and 100 ms abdominal impact were 10 hours, 45 minutes and 12 hours, 10 minutes respectively. Through the use of a living subject, comprehensive image data, and extensive geometric validation, this model has the potential to provide a greater degree of accuracy in blunt trauma simulations than existing human body models. It will serve as the foundation of a global effort to develop a family of next-generation computational human body models for injury prediction and prevention.

Introduction

Automotive injury has become a global public health problem, causing 1.2 million deaths and up to 50 million non-fatal injuries each year. [1] Motor vehicle crashes kill more people ages 5 to 34 than any other cause of death in the United States alone. [2] Computational human body models designed for vehicle occupant injury prediction provide a new tool that can offer insights into injury mechanisms and may lead to improved vehicle safety system design. This paper describes the development of a seated human body finite element model as part of the Global Human Body Models Consortium (GHBMC) project. Validation and benchmarking results for two cases are presented.

The GHBMC is an international consortium of automakers & suppliers working with research institutes and government agencies to advance human body modeling (HBM) technologies for crash simulations. The objective of the consortium is to consolidate world-wide human body model research and development into a single global effort. The role of the project's Integration Center of Expertise at Wake Forest University (WFU) was to; 1. Recruit subjects to serve as the template for model generation, 2. Acquire medical image and anthropometry data from recruited subjects, 3. Develop Computer Aided Design (CAD) data for meshing and FEA model development, and 4. To assemble Body Region Models (BRMs) that were meshed by partnering research universities within the consortium and validate the full body model. This paper reviews the work of the Integration Center at WFU and presents the 50th percentile seated male full body model (M50).

The M50 seated finite element male is intended for use in simulations of vehicle crash and was developed in LS-DYNA Rev. 4.2.1. The model has been developed to simulate kinematic and kinetic responses of the body in the blunt loading regime.

Methods: Medical Imaging and CAD Development

Detailed descriptions of the CAD development and external anthropometry data can be found in the literature. [3, 4] In this paper, we provide a brief overview of each. The subject recruited to serve as the M50 template was a 26 year old male, 78.6 kg, 174.9 cm and in excellent health. The subject matched target criteria based on an anthropometry survey by the U.S. Army [5] within an overall average of 5%. Imaging data were collected in three separate modalities; MRI (Magnetic Resonance Imaging), upright MRI and CT (Computed Tomography). External anthropometry data was collected in the seated posture using a three-dimensional digitizer (FARO Technologies Inc., Lake Mary, FL), Figure 1.



Figure 1. The M50 subject was recruited for the GHBM study after meeting extensive anthropomorphic criteria based on previous research. [5]

The image collection protocol was approved by the Wake Forest University School of Medicine Institutional Review Board (IRB). Supine MRI data were collected on a 1.5 Tesla Twin Speed scanner (GE, Milwaukee, WI). A three dimensional Fast Spoiled Gradient Recalled pulse sequence was used to facilitate segmentation of the images into various structures. The upright MRI protocol utilized a 0.6 Tesla Fonar Upright MRI (Fonar Inc., Melville, NY). Upright MRI was used to accurately capture bone and organ location and morphology when situated in a true seated posture. Three dimensional gradient echo pulse sequences similar to MRI were used for this modality. Computed tomography (CT) scans were acquired using a GE LightSpeed, 16-slice scanner, software revision 07MW11.10, service pack 2 (GE, Waukesha, WI). Images were acquired in helical mode, with the subject in the supine and an approximately seated position. Imaging modalities are reviewed in Figure 2.

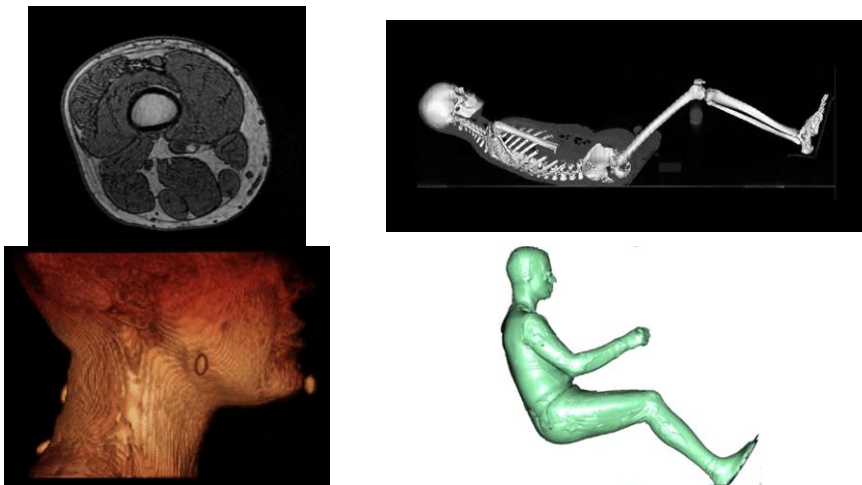


Figure 2. Overview of data collected for full body CAD development. Clockwise from upper left, conventional MRI thigh cross section, quasi-seated CT scan, external body laser scan in seat buck (raw point data), and upright MRI, lateral view of neck

After the acquisition of medical image data, the next major task was the development of CAD data of the human body. The first step in CAD development was segmentation, which was conducted by three primary means (Figure 3). Automatic segmentation was used in limited cases where atlas-based algorithms were available and was predominantly used to segment white and gray matter in the brain. A Semi-automated approach was used for bones where contrast between bone and surrounding tissue was large (in CT data). Finally, manual segmentation was required for most other soft tissues. A more complete description of the methods used is available in the literature. [3, 4]

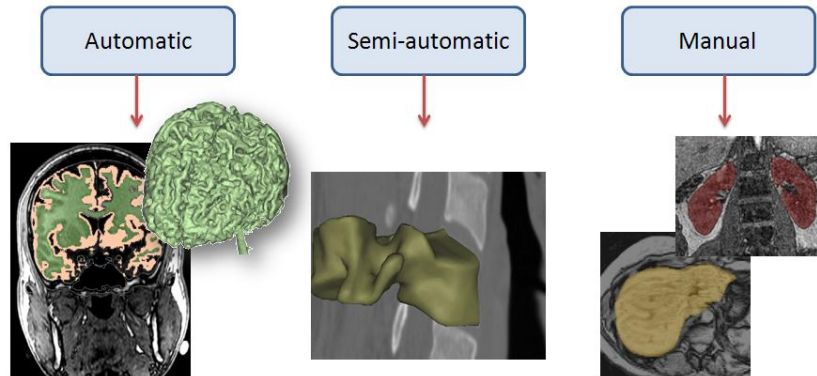


Figure 3. Segmentation overview for M50 model. Three types of segmentation were used, automatic, semi-automatic and manual.

Segmented data was conditioned to match the location and morphology of the organs in the upright MRI scans. NURBS (Non-Uniform Rational B-Spline) surfaces were developed on segmented polygon data. Border continuity was enforced such that the patchwork was tangentially continuous with neighboring patches. Parts on the midline are sagittally symmetric. For all components, the lowest number of splines per patch that still captured the contours of the underlying polygon model was used. [7] There are 418 individual CAD parts in the M50 model, including 179 individual bones (described with 216 parts), 46 organs and components thereof, 96 muscles, 37 vessels and 26 ligaments, tendons and other cartilaginous structures (Figure 4). The geometry of the model was generated predominantly from a recruited individual to serve as the 50th percentile male; however the anatomy was rigorously cross checked against literature values. [4]

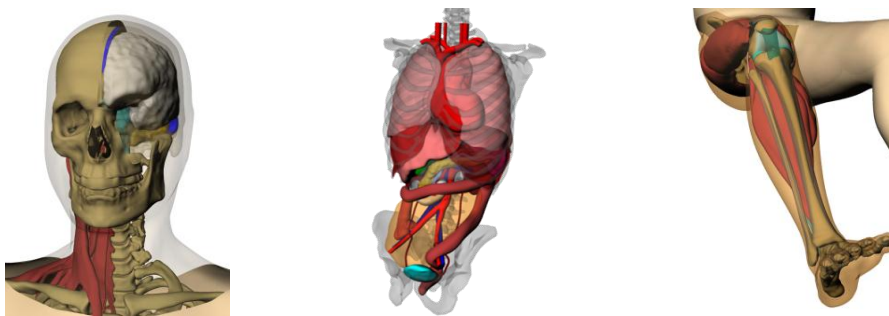


Figure 4. CAD data of M50, Left to right, detail of head and neck, detail of thorax and abdomen, detail of lower extremity.

Methods: Model Integration

Five Body Region Models (BRMs) were developed by partner research institutions in the GHBMC (Figure 5). The CAD data was meshed and regional models were validated. [6-11] These regional models were then transferred to the Integration Center to assemble the full body model. We briefly review model integration for each of the 4 interfaces below. Further detail can be found in Thompson et al. [12] Preprocessing was conducted using LS-PrePost (v. 3.1 LSTC) and HyperMesh (v. 11, Altair Inc., Troy, MI).

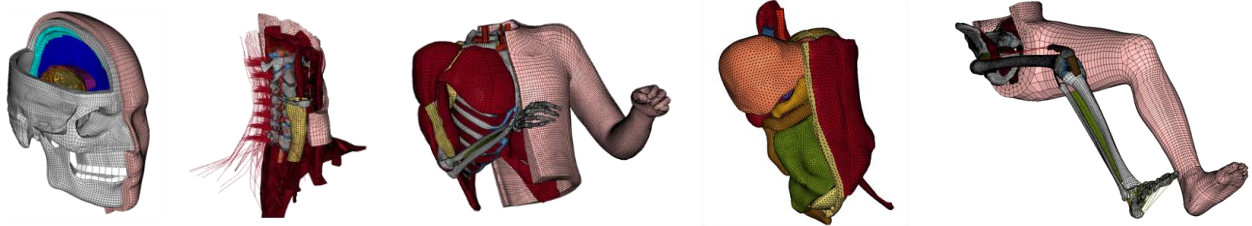


Figure 5. Body Region Models (BRMs). Left to Right, Head, Wayne State University (PI's K. Yang and L. Zhang), Neck, The University of Waterloo (PI, Duane Cronin), Thorax, University of Virginia (PI's R. Kent and D. Subit), Abdomen, IFSTTAR & Virginia Tech (PI's Philippe Beillas and Warren Hardy) and PLEX, The University of Virginia (Pelvis and Lower Extremity COE, PI's Costin Untaroiu, Jeff Crandall and Alan Eberhardt of the University of Alabama-Birmingham).

Head to Neck Interface – Cartilage on the skull required remeshing due to penetrating elements with C1. The hyoid bone, modeled as a rigid body, was attached to the skull through spring elements. Fifty two three-dimensional muscles that were modeled in the neck were attached to the skull and cervical vertebrae via tied contacts. Ligaments, fibers and all 1-dimensional elements (36 muscle and 8 ligamentous groups) were connected to the head model via nodal connections as well. The head and neck flesh was integrated through nodal connections. Remeshing was conducted to complete the connection between the brainstem and spinal cord (Figure 6). Flesh was connected with node to node continuity.



Figure 6. Head-Neck model integration. Left, lateral view of deep structures, Right, posterior view of neck muscles tied to skull.

Neck to Thorax Interface - All 1D neck muscles (n=62), 1D neck ligaments (n=4) and three-dimensional neck muscles (n=52) were attached to the corresponding thoracic bony landmarks. Tied contacts were used for the 3D muscles (Figure 7). The superior facet of T1 was modified for node to node agreement with the neck model. The thorax and neck flesh components were connected through shared nodes. One dimensional ligamentous connections from the neck model along the cervical spine were connected to T1.



Figure 7. Neck-Thorax and Thorax-Abdomen model integration. Left to right: posterior view of back musculature, anterior view, anterior view of heart and great vessels, posterior view.

Thorax to Abdomen Interface – Tied contacts between thoracic and abdominal muscles to their neighboring regions were established (i.e. rectus abdominis and obliques to ribs, Figure 7). Abdominal ligaments were connected via shared nodes to the inferior surface of the diaphragm. The thoracic and abdominal great vessels were attached through shared nodes. Superior lumbar kinematic constraints were confirmed. Both the thoracic and lumbar spinal vertebrae are modeled as rigid bodies.

Abdomen to Pelvis and Lower extremity Interface - Tied contacts between abdominal and thoracic muscles to the pelvis and lower extremity bones were made (Figure 7 and Figure 8). The lumbar spine was integrated using a rigid plate. The plate constrains the L5-S1 kinematic joint beam nodes from the abdomen COE to the deformable sacrum. Contacts between components of the inferior abdominal cavity and pelvic rim were established.

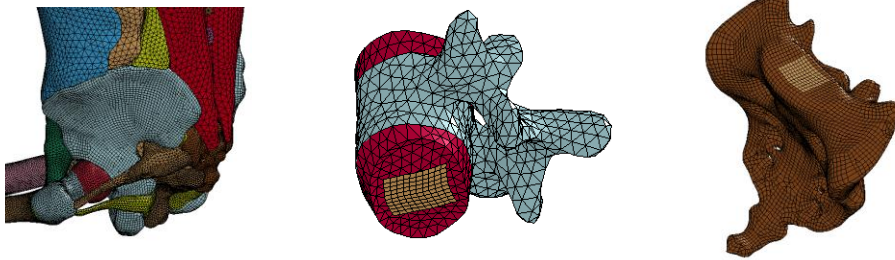


Figure 8. Abdomen-Plex Model integration. Right, muscles with tied contacts. Middle, left, plate used to constrain the lumbar spine to the sacrum.

The integration center was responsible for modeling the soft tissue flesh envelope surrounding the full body model. The current implementation uses a simplified rubber model (Mat. 181) in which the tension is based on the tensile loading from the sartorius muscle data from Yamada [13], and the compression data is based on the force vs. deflection response of the simulated block compression test, using material data from Untaroiu [14].

Methods: Model Validation and Benchmarking

The M50 model has been tested in nearly 20 impact simulations in frontal and lateral loading. A subset of these that have also been benchmarked on a high performance cluster computer are presented. The first case presented is a frontal hub impact using a 23.4 kg impactor moving at 6.7 m/s, contacting the chest at mid-sternum. [15] This is a free back loading condition. The second simulates a 48 kg rigid bar impact at the level of the umbilicus moving at 6 m/s. [16] This test is also a free back loading condition.

Publicly accessible databases are available for benchmarking crash simulations in commercial finite element codes, such as TopCrunch.org. However, most benchmarks for crash simulations are based on automotive models with different mesh, material, and contact definitions than computational human body models. Therefore the M50 model was tested to provide initial data on processor scalability, performance, and multiprocessor efficiency in the above blunt loading scenarios, using a high-performance computing cluster. The Wake Forest University DEAC Cluster was used for computing model simulations using massively parallel processing (MPP) versions of LS-DYNA 971 R4.2.1 (LSTC, Liverpool, CA). These two simulations were chosen because they are commonly loaded regions in motor vehicle crash, and the impacts occur in geometrically complex regions.

The current DEAC cluster features a collection of IBM Blade Centers with 182 nodes comprising over 1400 Xeon cores running on a Red Hat Enterprise Linux operating system. Typical configurations of each node include 2.33-2.66Ghz Xeon E series processors with 16 to 48 GB of installed RAM utilizing Infiniband and Ethernet nodal interconnects. A controlled time step of 0.3 μ s was imposed. The model was tested using up to 88 CPUs and computational times were recorded.

Results: The M50 Seated Occupant Full Body Model

Summary statistics of the M50 model are found in Table 1. The mass distribution by region is found in Figure 9 and a picture of the integrated model can be found in Figure 10. The largest region by both element count and mass is the Pelvis and Lower extremity region comprising roughly 50% of the mass and a third of the elements (Figure 11). The Neck model contains roughly 260×10^3 elements due to modeling each neck muscle with solid hexahedral elements (Figure 6, Figure 7, Figure 10, and Figure 11). Element types used in the model are summarized in Figure 12. The most common element type is solid hexahedral, comprising 41% of the model. The M50 brain, thorax, and lower extremity are majority hexahedral elements. Many soft tissue structures within the abdomen are modeled with solid tetrahedral elements (the second largest element component at 33.8%).

Table 1. FBM 3 Model Summary statistics

Number of Elements / Nodes	$1.95 \times 10^6 / 1.30 \times 10^6$
Number of Parts	847
Number of Materials	557
LS-DYNA build used to test model for validation	R 4.2.1 Rev.: 53450 Prod. ID: 54013
MPP on high performance cluster computer	mpp971_s_R4.2.1_Intel_linux86-64_hpmpi
Model Mass (kg)	75

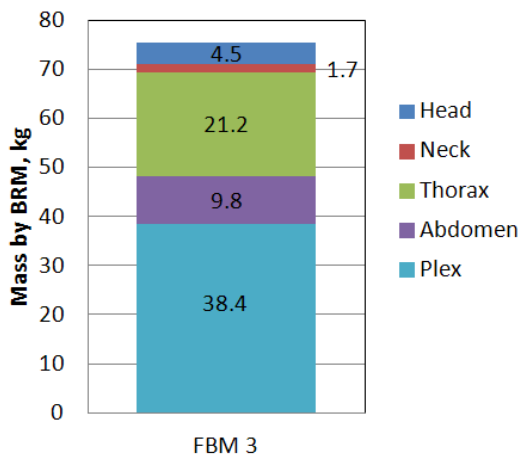


Figure 9. Model mass distribution by BRM showing the total mass for each region.



Figure 10. Oblique view of the M50 model, seated, with the flesh layer blanked on half to show underlying structures.

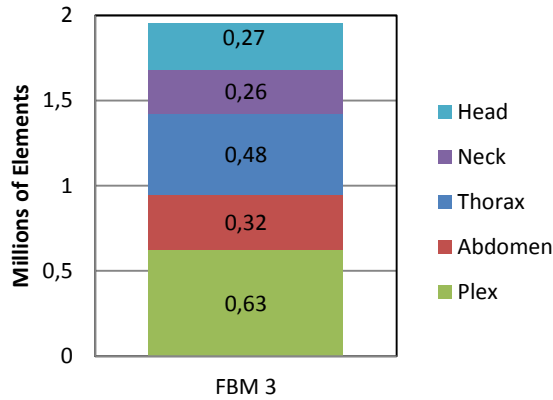


Figure 11. Element breakdown by BRM within the FBM model.

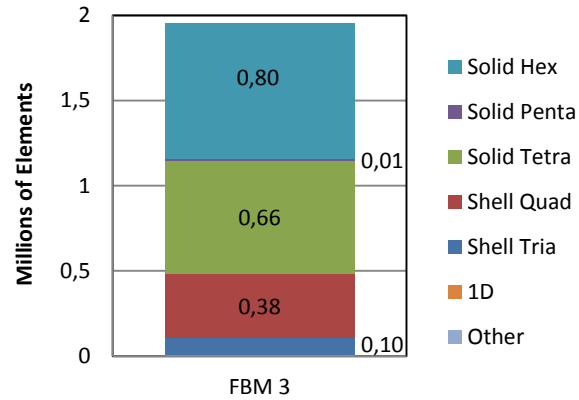


Figure 12. Element breakdown by element type within the FBM model.

Hard target element quality standards were set for the Jacobian and tetrahedral collapse criterion. The goal for these “hard targets” was to have 100% adherence to the standards, which were: Jacobian greater than 0.4 for shells (quadrilateral and tria) and greater than 0.3 for solid hex elements. Tetrahedral collapse was to be kept greater than 0.2. Broadly, all regions met this goal, with noncompliance below 0.005% in all regions. Additional element quality specifications were applied, with a maximum non-compliance of 1% for all regions.

The M50 model contains detailed anatomy in each body region which we briefly summarize here, first reviewing bone data, then soft tissue data. Layers of the skull bone are modeled individually with hex elements, including the diploë. The neck model contains all relevant bony anatomy including cervical vertebral bodies and the hyoid bone. Long bones in the upper extremity of the model including the humerus, radius, ulna and clavicle use hexahedral elements for trabecular bone and shell elements for cortical bone. Long bones in lower extremity of the model use solid hexahedral elements for cortical bone in the midshaft, while the cortical bone in the epiphyseal ends of these bones is modeled with shell elements. Trabecular bone in these cases is modeled with hexahedral elements. The pelvis is modeled with solid hexahedral cortical bones and solid tetrahedral elements for trabecular bone. Ribs are modeled with shell elements for cortical bone and solid hexahedral for cancellous bone. Rib thickness varies regionally. Fracture of the ribs is modeled through the use of piecewise linear plasticity with failure. [17]

The head model contains 17 sub structures of the brain including the white and gray matter, CSF, sinuses, cerebellum, basal ganglia, corpus callosum and ventricles. The tentorium, falx, pia and dura are modeled with shell elements. Neck ligaments are modeled as one-dimensional elements with progressive failure. Facet joints, the annulus fibrosus and nucleus pulposus are also included in the model. The 52 muscles of the neck region are also modeled as three-dimensional hexahedral structures with one-dimensional elements within them. Thorax model contains the heart, lungs, diaphragm and great vessels. Fat pads are used as void filling structures. A number of thoracic muscles relevant to blunt loading are also included such as the pectoralis major, deltoid, biceps, triceps. The abdomen model contains all major soft tissue organs and vessels including the liver, spleen, kidneys, colon, small bowel, bladder, inferior vena cava, portal vein, descending aorta, and relevant vascular tethers to organs. Muscles of the abdomen including the rectus abdominis, obliques, erector spinae, and quadratus lumborum are modeled as 3-

dimensional structures. In the Plex region, muscles of the pelvic rim including the psoas, iliac, piriformis, obturator internus and levator ani are modeled. Within the lower extremity, the knee ligaments including the MCL, LCL, PCL, ACL, menisci, quadriceps tendon and patellar tendon are modeled.

Thus, a large number of distinct anatomical structures were modeled explicitly rather than homogenizing the body's anatomy. A consequence of this approach is that the model contains void space since not all structures could be modeled. However, this void space accounts for only 4.2% of the total model volume. More than half of the void is found in the thorax, abdomen, and pelvis. Because the mass distribution is extremely important to the kinematics of the model, the location of body segment centers of gravity were thoroughly documented and compared against previous studies, showing good agreement. [18] The origin of the global coordinate system for the FBM model is located at the H-point of the seat buck. This location corresponds to the central pelvis of the model. A world coordinate system, defined per the SAE J1733 sign convention, was aligned to the mid-sagittal plane. The positive x-direction points anteriorly, the positive y-direction points to the model's right, and the positive z-direction points inferiorly to make a right-handed coordinate system. The model is pre-programmed with a number of output node sets such as head, shoulder, hip and knee photo-targets for tracking kinematics.

Validation and Benchmarking Results: M50 Seated Occupant Model

The results from the validation simulations are shown below in Figure 13 and Figure 14. Figure 13 shows time sequences of these two impacts on the M50 model with transparent flesh to show the loading on the underlying structures.

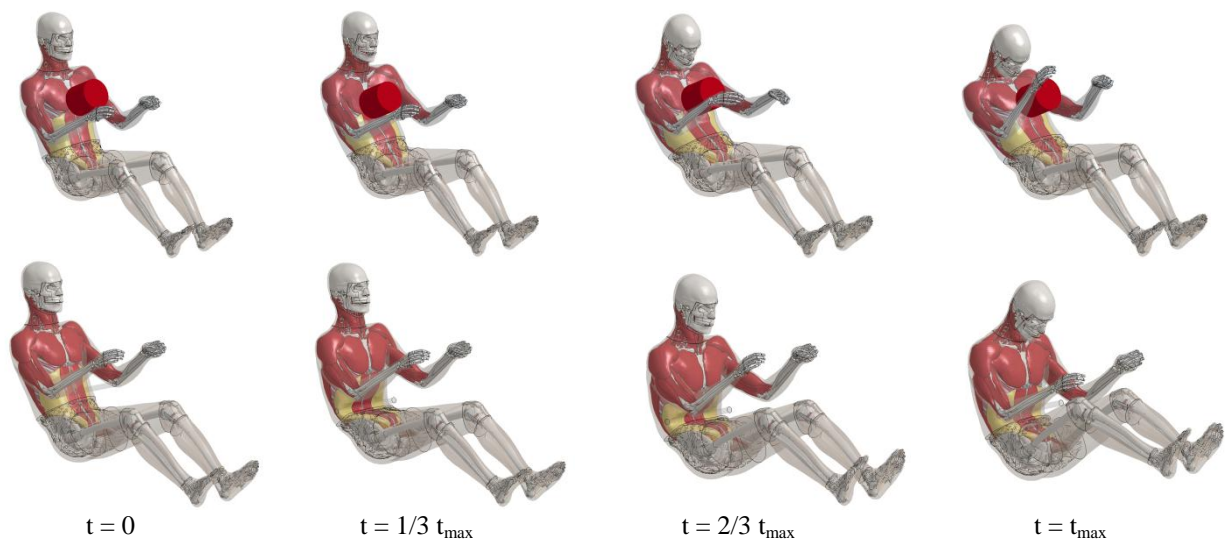


Figure 13. Time lapse sequence of model impacts, chest impact per Kroell [15] (Upper) and abdominal bar impact per Hardy (Lower) [16]

The impact force vs. deflection traces are shown in Figure 14 for both impacts. The chest impact is shown with corridors from Neathery et al.'s analysis of Kroell's data. [15] The response of the anterior loading of the thorax appears stiff with slightly greater than expected peak force and lower than expected sternal deflection. No Rib fractures were noted in these simulations.

Interestingly, while many of the PMHS tests used to develop these corridors exhibited multiple rib fractures, the two youngest specimens (aged 19 and 29) did not. The subject used in the development of the GHBM model was a 26 year old, which perhaps suggests a correlation.

The impact force vs. anterior deflection is shown for the abdominal bar impact in Figure 14 as well. Due to specimen differences, the plot for this test was modified from the paper to normalize displacement as displacement anterior to the spine only. Beillas et al. made this modification because of large scale differences in the anterior-posterior breadth of the subjects tested in [16] and the M50 model. [10] Once accounting for these differences, the response of the impact on M50 compares favorably with the experimental data.

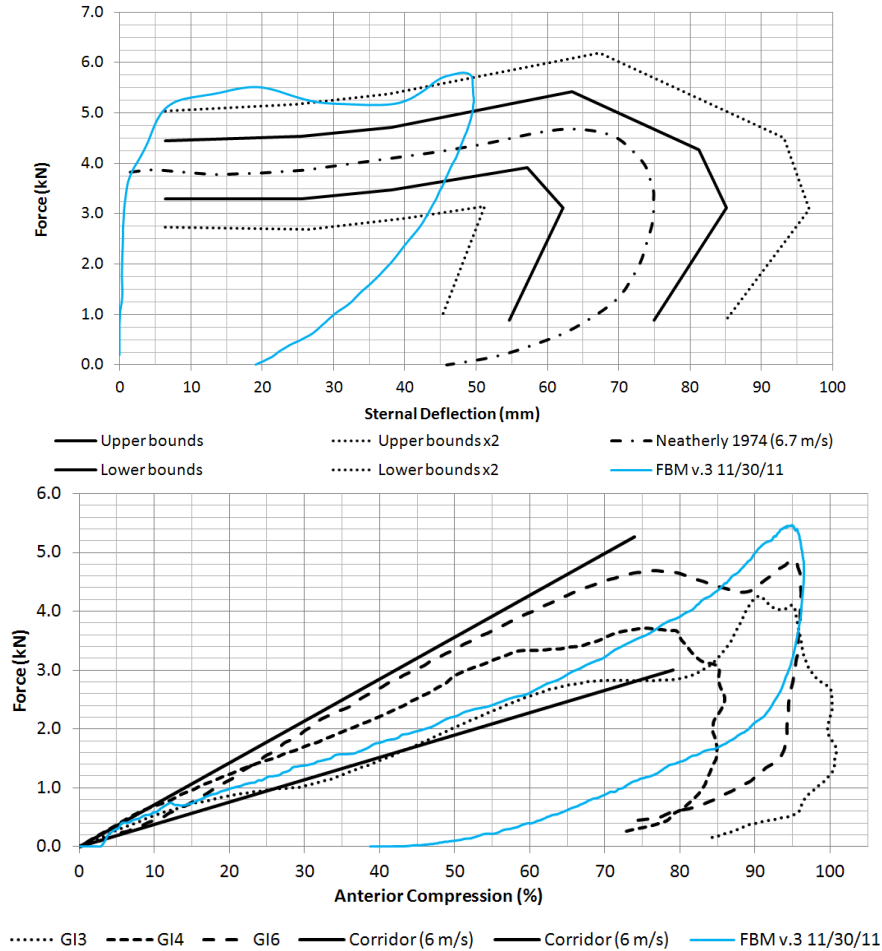


Figure 14. FBM 3 validation results, chest impact per Neatherly and Kroell at 6.7 m/s [15] (upper) and abdominal bar impact per Hardy [16] (lower). Results plotted vs. anterior compression per methods of Beillas et al. [10]

Results from the benchmarking study are shown in Figure 15. The performance of each simulation was characterized by the number of processors and the type of nodal interconnect. It should be noted that the chest impact simulation duration was 60 ms whereas the abdomen impact simulation duration was 100 ms. A performance gain is clear when using infiniband interconnects, in particular in the abdomen impact, which shows 32 hours vs. 12 hours with 64 cores. Scalability gains drop off after roughly 80 CPU's on the abdomen impact, but a similar increase was not found with the chest impact at the same number of CPU's. Despite its longer

simulation time, the abdomen requires roughly same time to compute as the chest impact after 64 CPU's. A large portion of the computational time was found to be spent on contact algorithm processing.

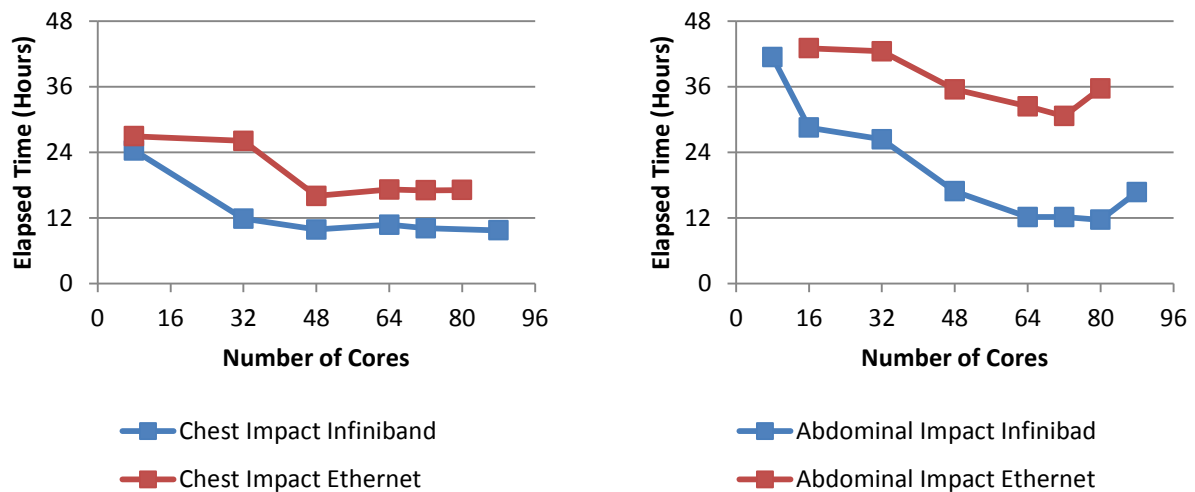


Figure 15. Benchmarking data for the Chest Impact (right) and Abdomen Impact (left).

Discussion

Advanced human body models are expected to enhance the injury assessment and research capabilities of biomedical engineers studying blunt trauma. The M50 model is unique in that its geometry is based on medical image data collected for the expressed purpose of developing a full body finite element model. Therefore, the M50 seated occupant is perhaps the best anatomical portrayal of the human seated posture to date in a full body finite element model.

The model has been tested in a number of different impact loading scenarios with good biofidelity observed in nearly all scenarios. Recent model enhancement work by the Integration Center has improved robustness. Future work will focus on continued enhancement of the model, improving the goodness of fit vs. literature studies and quantifying its deviation for these studies. This work will include improving matched literature tests by focusing on the model's posture, perhaps through gravity settling into the various bucks, and test setups used to validate the model.

The benchmarking study provided initial guidance for expected simulation efficiency when running the M50 model. The model showed good scalability gains through 64 CPUs and up to 80 CPUs when utilizing infiniband interconnects. A lower effectiveness is shown using Ethernet connections with more processors due to the elevated nodal communication costs. A large portion of the computational time was found to be spent on contact algorithm processing suggesting improving contact efficiency as a potential task for further model enhancement.

Summary

The seated M50 model is the first to be developed and validated by the Global Human Body Models Consortium and concludes Phase I efforts. Six centers of expertise at research

universities contributed to the model development effort, with Wake Forest University performing model integration tasks. The M50 model has 1.9 million elements, 1.3 million nodes, and weighs 75 kg. Extensive validation has been conducted at the FBM level. Initial model development was conducted in LS-DYNA. Continued work via the consortium will focus on further enhancement of the M50 model, development of small female and large male models

Acknowledgements

Funding support was provided by the Global Human Body Models Consortium, LLC through grant WFU: FBM-001. The authors gratefully acknowledge the contributions of the Body Region Centers of Excellence (COE) in the GHBMC model development at the regional level. This work was conducted by Wayne State University (Head COE, PI's King Yang and Liying Zhang), The University of Waterloo (Neck COE, PI Duane Cronin), The University of Virginia (Thorax COE, PI's Richard Kent and Damien Subit), IFSTARR & Virginia Tech (Abdomen COE, PI's Philippe Beillas and Warren Hardy) and The University of Virginia (Pelvis and Lower Extremity COE, PI's Costin Untaroiu and Jeff Crandall and Alan Eberhardt at the University of Alabama-Birmingham). Dr. Untaroiu is currently faculty at Virginia Tech. The authors also acknowledge Timothy Miller and David Chin for support with the DEAC Computational cluster.

References

1. WHO, *Global status report on road safety: time for action*. Geneva, 2009 (http://whqlibdoc.who.int/publications/2009/9789241563840_eng.pdf). 2009.
2. Gayzik, F.S., et al., *A finite element-based injury metric for pulmonary contusion: investigation of candidate metrics through correlation with computed tomography*. Stapp Car Crash J, 2007. **51**: p. 189-209.
3. Gayzik, F.S., et al., *External Landmark, Body Surface, and Volume Data of a Mid-Sized Male in Seated and Standing Postures*. Ann Biomed Eng, 2012.
4. Gayzik, F.S., et al., *Development of a full body CAD dataset for computational modeling: a multi-modality approach*. Ann Biomed Eng, 2011.
5. Gordon, C., et al., *1988 Anthropometric Survey of U.S. Army Personnel: Methods and Summary Statistics*, D.a.E.C. Prepared for United States Army Natick Research, Editor. 1989.
6. Fice, J.B., D.S. Cronin, and M.B. Panzer, *Cervical spine model to predict capsular ligament response in rear impact*. Ann Biomed Eng., 2011. **39**(8): p. 2152-62.
7. Li, Z., et al., *Influence of mesh density, cortical thickness and material properties on human rib fracture prediction*. Med Eng Phys, 2010. **32**: p. 998-1008.
8. Li, Z., et al., *Rib fractures under anterior-posterior dynamic loads: experimental and finite-element study*. J Biomech, 2010. **43**(2): p. 228-34.
9. Yue, N., J. Shin, and C.D. Untaroiu, *Development and Validation of an Occupant Lower Limb Finite Element Model*. SAE Technical Paper, 2011.
10. Beillas, P. and F. Berthet, *Performance of a 50th percentile abdominal model for impact: effect of size and mass*, in *European Society of Biomechanics Conference*. 2012: Lisbon, Portugal.
11. DeWit, J.A. and D.S. Cronin, *Cervical spine segment finite element model for traumatic injury prediction*. Journal of the Mechanical Behavior of Biomedical Materials, 2012. **10**(0): p. 138-150.

12. Thompson, A.B., et al., *A paradigm for human body finite element model integration from a set of regional models*, in *Biomed Sci Instrum.* 48. 2012: Blacksburg, VA.
13. Yamada, H., *Strength of Biological Materials*, ed. F. Evans. 1970, Baltimore: Williams and Wilkins Company.
14. Untaroiu, C., et al., *A finite element model of the lower limb for simulating pedestrian impacts*. Stapp Car Crash J, 2005. **49**: p. 157-81.
15. Neathery, R., *Analysis of Chest Response Impact Data and Scaled Performance Recommendations*. Stapp Car Crash J, 1974. **18**: p. 459-493.
16. Hardy, W.N., L.W. Schneider, and S.W. Rouhana, *Abdominal impact response to rigid-bar, seatbelt, and airbag loading*. Stapp Car Crash J, 2001. **45**: p. 1-32.
17. Li, Z., et al., *Rib fractures under anterior-posterior dynamic loads: Experimental and finite-element study*. Journal of Biomechanics, 2010. **43**: p. 228.234.
18. Thompson, A.B., et al., *Methods for validation of the mass distribution of a full body finite element model - biomed 2011*. Biomed Sci Instrum. **47**: p. 100-5.

